Materials Letters 281 (2020) 128638

Contents lists available at ScienceDirect

Materials Letters

journal homepage: www.elsevier.com/locate/mlblue

# Epitaxial growth of polarization-graded AlGaN-based solar-blind ultraviolet photodetectors on pre-grown AlN templates

Yiren Chen, Zhiwei Zhang, Guoqing Miao, Hong Jiang, Zhiming Li, Hang Song *

*State Key Laboratory of Luminescence and Applications, Changchun Institute of Optics, Fine Mechanics and Physics, Chinese Academy of Sciences, Changchun 130033, China*

ARTICLE INFO

*Article history:*
Received 19 June 2020
Received in revised form 30 August 2020
Accepted 3 September 2020
Available online 12 September 2020

*Keywords:*
Epitaxial growth
Sensors
AlGaN
Solar-blind ultraviolet
MOCVD

ABSTRACT

In this letter, based on the method of introducing one mesothermal AlN (MT-AlN) interlayer, a high-quality AlN template is firstly obtained by adjusting the growth rate of the high-temperature AlN (HT-AlN) epilayers on both sides of the MT-AlN interlayer. Then, the epitaxial growth of polarization-graded AlGaN-based solar-blind ultraviolet photodetector (SUV-PD) structural material is implemented on the pre-grown AlN template by introducing an n-$Al_xGa_{1-x}N$ gradient layer. It leads to the elimination of band discontinuity and forms a polarization-graded induced field resulting in a high-performance back-illuminated AlGaN-based SUV-PD. This research provides an important reference for the development of high-performance back-illuminated AlGaN-based SUV-PDs.



## 1. Introduction

Because of the potential applications in both military and civil fields, such as early missile approach warning for important military targets, corona leakage detection for ultra-high voltage (UHV) and high voltage (HV) power grids, free-space optical communication for confidential information, chemical/biological agent sensing for public health & biosecurity, and so on [1–3], there is drawing considerable attention and interest in SUV-PDs. Due to its direct wide and tunable bandgap, all-solid-state, filter-free and anti-radiation nature, the ternary AlGaN alloy is considered to be one of the most ideal materials for developing SUV-PDs, and the development of high-performance SUV-PDs based on AlGaN is expected to provide a promising alternative to conventional photomultiplier tubes (PMTs) or Si-based photodiodes relied on additional complex deep ultraviolet band-pass filters [4]. However, the performance of the AlGaN-based SUV-PDs is impeded by the crystalline quality of high Al-content AlGaN under existing mainstream heteroepitaxial growth method, e.g. a large density of dislocations and a large number of cracks. The preparation of high-quality AlN templates as ideal substrates for growing high Al-content AlGaN materials and the optimal design of device structure can be effective ways to obtain high-performance AlGaN-based SUV-PDs.

Herein, the epitaxial growth of back-illuminated AlGaN-based SUV-PD material is implemented by two independent processes. One is the growth of AlN template. Based on the method of introducing one MT-AlN interlayer demonstrated in our previous research [5], the growth rate of the HT-AlN epilayers on both sides of the MT-AlN interlayer is modulated by adjusting the Ⅴ/Ⅲ ratio to further improve the quality. The other is the growth of PIN structure AlGaN-based SUV-PD material on the pre-grown AlN template. An n-$Al_xGa_{1-x}N$ gradient layer with Al-content gradually changing is introduced to construct built-in polarization in PIN structure to enhance its photoelectric conversion so that a high-performance back-illuminated AlGaN-based SUV-PD is achieved.

## 2. Experimental procedure

The epitaxial growth was implemented on a 2 in. double-side polished (DP) c-plane sapphire substrate by low-pressure metal-organic chemical vapor deposition (LP-MOCVD, Aixtron 200/4-HT). The cross-sectional image of the AlN template was obtained by a scanning electron microscope (SEM, Hitachi S4800). The rocking curves and the asymmetrical reciprocal space mapping (RSM) image around (1 0 $\bar{1}$ 5) reflection of the epitaxial materials were measured by high-resolution X-ray diffractometer (HRXRD, Bruker D8). The surface morphology of the AlN template was characterized by an atomic force microscope (AFM, Veeco multi-mode) in the tapping mode. An *in-situ* optical monitoring system (LayTec AG) was used to record the reflectance and temperature during the growth. The current-voltage (*I-V*) characteristics of the SUV-

* Corresponding author.
*E-mail address:* songh@ciomp.ac.cn (H. Song).

https://doi.org/10.1016/j.matlet.2020.128638
0167-577X/

PD were measured by a semiconductor parameter analyzer (Agilent B1500A). The spectral response properties of the SUV-PD were evaluated by a calibrated UV spectral response test system with a 300 W xenon lamp and a monochromator.

## 3. Results and discussion

Fig. 1(a) presents the schematic of the AlN template and its cross-sectional SEM image. The AlN epilayer is composed of four sub-layers, low-temperature AlN (LT-AlN) nucleation layer, high-temperature/high growth rate AlN layer (HT/HR-AlN), MT-AlN, and high-temperature/low growth rate AlN layer (HT/LR-AlN) with a total thickness of 1.9 μm. The corresponding 405-nm-wavelength *in-situ* growth reflectance curve is shown in Fig. 1(b). Prior to the growth, the sapphire substrate is thermally desorbed at 1200 °C under the mixture of $H_2$ and $NH_3$ to form an N-rich polar surface. Through adjusting the Ⅴ/Ⅲ ratio, a 270-nm-thick HT/HR-AlN epilayer is grown at a rate of 0.3 nm/s while a 1.52-μm-thick HT/LR-AlN epilayer is grown at a rate of 0.12 nm/s. The AlN template is finally cooling down to room temperature. For detailed growth information, it can be referred to in Supporting Information. In Fig. 1(c), it shows the AFM surface morphology of the AlN with a scan area of 20 × 20 $\mu m^2$ which presents clear atomic steps without any V-type defects or hillocks. The root mean square (RMS) roughness is evaluated as 0.556 nm. The full width at half maximum (FWHM) values of rocking curves for (0 0 0 2) and (1 0 $\bar{1}$ 2) planes (Fig. 1(d)) are 73 and 707 arcsec, respectively. The FWHM values of (0 0 0 2) and (1 0 $\bar{1}$ 2) planes are widely used to estimate the screw and edge dislocations in the heteroepitaxial material, originating on the broadening of the FWHM related to misorientations of crystallites [6]. The screw and edge dislocation densities can be evaluated as 1.16 × $10^7$ $cm^{-2}$ and 5.15 × $10^9$ $cm^{-2}$ by the method reported in Ref. [7], which indicates high crystalline quality of the AlN template.

Based on the pre-grown AlN template, a PIN structure AlGaN-based SUV-PD material is designed and epitaxially grown. Fig. 2 (a) and (b) show its 405-nm-wavelength *in-situ* growth monitoring curve and schematic configuration, respectively. A ten-period of $Al_{0.58}Ga_{0.42}N$/AlN (6 nm/6 nm) superlattices (SLs) layer is firstly deposited to suppress the dislocations extension from AlN to the subsequent epilayers and to release the strain accumulated by the heterogeneous mismatches [8]. Then, a 200-nm-thick intrinsic $Al_{0.58}Ga_{0.42}N$ (i-$Al_{0.58}Ga_{0.42}N$) epilayer is grown on top of the SLs. It is followed by the growth of PIN structure AlGaN-based materials (seen in Supporting Information for details). The n-$Al_{0.54}Ga_{0.46}N$ as a window layer has a higher Al-content than the absorption layer (i-$Al_{0.44}Ga_{0.56}N$) to enable back-illumination. Between n-$Al_{0.54}Ga_{0.46}N$ and i-$Al_{0.44}Ga_{0.56}N$, an n-$Al_xGa_{1-x}N$ gradient layer with the Al-content gradually changing from 0.54 to 0.44 is deposited to form graded polarization so as to eliminate the band discontinuity. The p-type AlGaN layer is composed of a p-$Al_{0.37}Ga_{0.63}N$ layer and a p-$Al_xGa_{1-x}N$ gradient layer with the Al-content gradually changing from 0.37 to 0.2 which is beneficial to improve its electrical contact. The carrier concentrations for the n-$Al_{0.54}Ga_{0.46}N$ and p-$Al_{0.37}Ga_{0.63}N$ layers are respectively evaluated to be 1.0 × $10^{18}$ $cm^{-3}$ and 1.2 × $10^{17}$ $cm^{-3}$ by an electrochemical capacitance-voltage (ECV) method based on the epitaxial wafer instead of Hall measurement [9–11].

The asymmetrical RSM around (1 0 $\bar{1}$ 5) reflection of the epitaxial material is presented in Fig. 2(c). The reciprocal lattice points (RLPs) shown in RSM are well consistent with the material structure of Fig. 2(b). The introduction of a thin n-$Al_xGa_{1-x}N$ gradient layer marked by a white circle not only plays a role of regulating the strain in the heterogeneous materials, but also creates a polar-

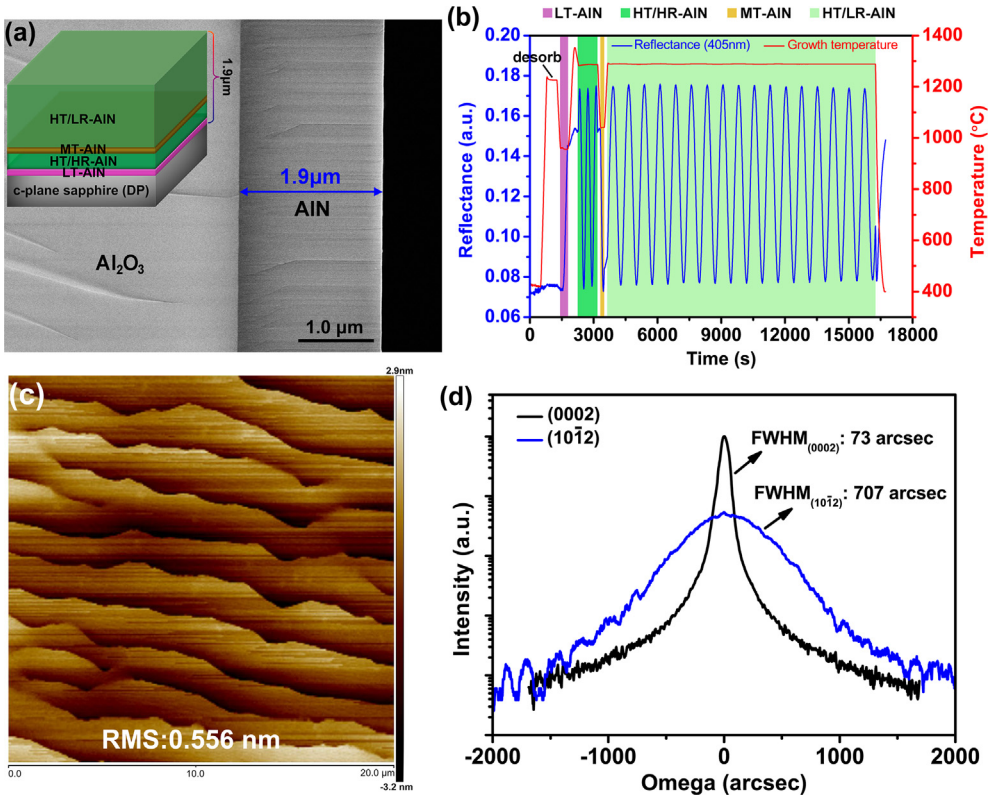


**Fig. 1.** (a) Schematic of the AlN template (inset) and its cross-sectional SEM image. (b) The 405-nm-wavelength *in-situ* growth monitoring curve. (c) AFM surface morphology of AlN with a scan area of 20 × 20 $\mu m^2$ and (d) The rocking curves of (0 0 0 2) and (1 0 $\bar{1}$ 2) planes for the AlN template.

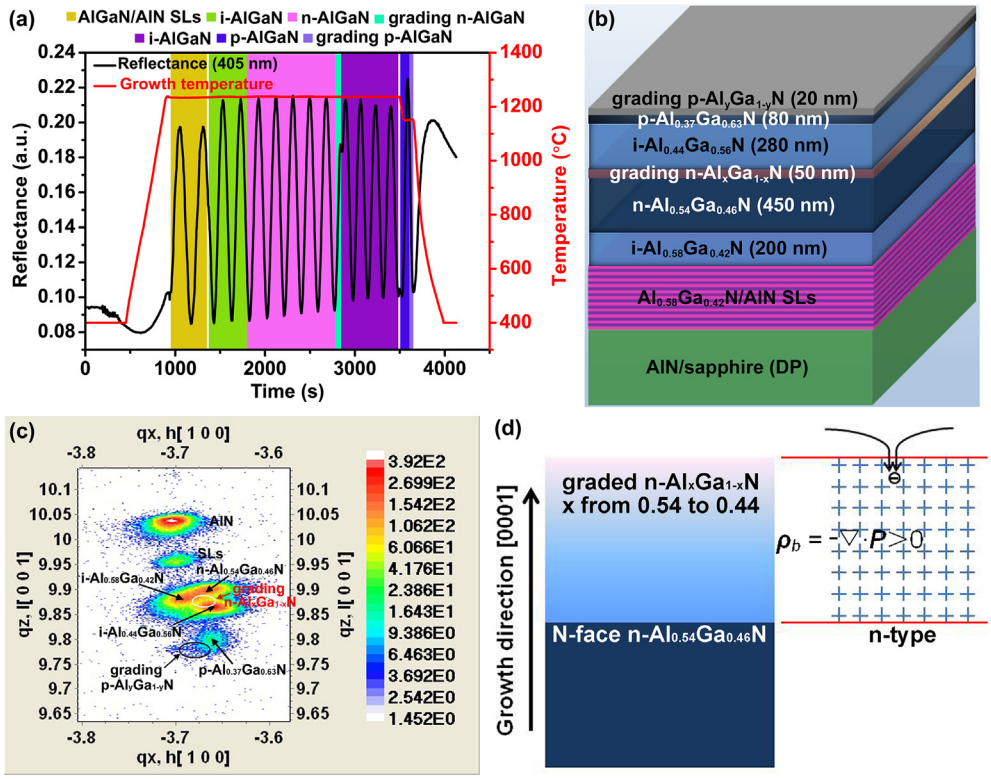


**Fig. 2.** (a) The *in-situ* growth monitoring curve for the PIN structure AlGaN-based SUV-PD. (b) Schematic configuration and (c) Asymmetrical RSM around (1 0 $\bar{1}$ 5) reflection of the epitaxial material. (d) The positive polarization charge field created by grading n-$Al_xGa_{1-x}N$ on N-face n-AlGaN.

ization charge field. Differing from the metal-face polar growth in the [0 0 0 1] direction [12], the special surface nitriding treatment is used to realize N-face polar growth in this paper. As shown in Fig. 2(d), for N-face polar growth along the [0 0 0 1] direction, when the Al-content linearly changes from 0.54 to 0.44, a linear change in the polarization occurs in the n-$Al_xGa_{1-x}N$ gradient layer, resulting in a fixed positive space charge. The positive charge field will attract the bound sheet negative charges formed at the heterogeneous interface [13] and the photon-generated electrons generated by illumination. As a result, it reduces the photon-generated carriers' loss due to reflection or trapping at the abrupt heterojunction and improves their separation, transmission and collection so as to achieve high-performance back-illuminated AlGaN-based SUV-PDs.

In order to reveal the performance of the AlGaN-based SUV-PD material, a back-illuminated photodetector with a 300-μm-diameter photosensitive mesa is prepared for evaluation. The detailed fabrication process can be found in our previous related research [8]. The schematic and physical images of the device are shown in Fig. 3(a). The dark *I-V* curve in Fig. 3(b) shows good rectifying behavior with a current density of $3.9 \times 10^{-8}$ A/mm$^2$ at −5 V. The measured spectral responsivities and corresponding EQEs under different bias are demonstrated in Fig. 3(c) and (d), respectively. The response spectra present bandpass feature in the solar-blind UV region ranging from 260 nm to 290 nm, with a peak located at 274 nm. The response spectrum of UV-enhanced standard Si-PD (black line in Fig. 3(c)) is used for comparison. Obviously, the spectral responsivity of the AlGaN-based SUV-PD is significantly greater than that of standard Si-PD in the solar-blind UV band, whether bias is applied or not. The peak responsivity and corresponding EQE at zero-bias are measured as 172.7 mA/W and 78.1% while 204.5 mA/W and 92.6% for 5 V reverse bias, and the ultraviolet/visible rejection ratio is more than three orders of magnitude. As the reverse bias increases, the responsivity starts to increase a lot and then flattens out. The inset of Fig. 3(d) shows the variation trend of EQE with applied bias voltage, indicating the limit EQE is going to be 95%.

## 4. Conclusions

The epitaxial growth of AlGaN-based SUV-PD material is carried out by two separate processes using LP-MOCVD. The growth rate modulation method is adopted to further improve the quality of the AlN template based on the method of introducing one MT-AlN interlayer while an n-$Al_xGa_{1-x}N$ gradient layer is introduced in the PIN structure AlGaN-based SUV-PD material to construct a polarization-graded induced field. As a result, the related device exhibits a low dark current density and a high spectral response characteristic with an upper limit EQE estimated to be 95%. The polarization-graded n-$Al_xGa_{1-x}N$ epilayer plays a role of reducing the loss of the photon-generated carriers due to reflection or trapping at the abrupt heterojunction and improving carrier separation and transmission, which is beneficial to develop high-performance back-illuminated AlGaN-based SUV-PDs.

## CRediT authorship contribution statement

**Yiren Chen:** Conceptualization, Methodology, Data curation, Writing - original draft, Funding acquisition. **Zhiwei Zhang:** Methodology, Investigation. **Guoqing Miao:** Validation, Resources. **Hong Jiang:** Project administration, Resources. **Zhiming Li:** Investigation, Visualization. **Hang Song:** Supervision, Funding acquisition.

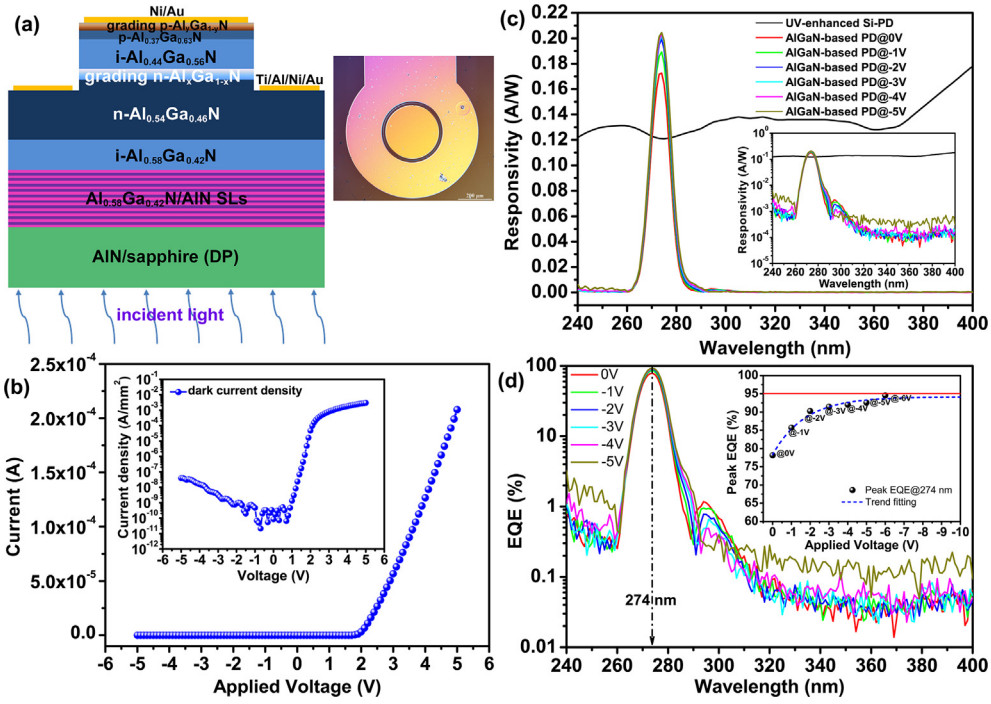


**Fig. 3.** (a) Schematic and physical images of the back-illuminated PIN structure AlGaN-based SUV-PD. (b) The dark *I-V* curve and the corresponding current density (inset) of the device. (c) Measured spectral responsivities under different bias in contrast with that of UV-enhanced standard Si-PD. The inset shows the responsivity plot in semi-log scale. (d) The corresponding EQE in semi-log scale. The inset shows the variation trend of EQE with applied bias.

## Declaration of Competing Interest

The authors declare that they have no known competing financial interests or personal relationships that could have appeared to influence the work reported in this paper.

## Acknowledgments

This work was partially supported by National Natural Science Foundation of China (Grant Nos. 61504144 and 51472230), and Department of Science and Technology of Jilin Province (Grant No. 20170520156JH).

## Appendix A. Supplementary data

Supplementary data to this article can be found online at https://doi.org/10.1016/j.matlet.2020.128638.

## References

[1] R. McClintock, M. Razeghi, Proc. SPIE 9555 (2015) 955502.
[2] J. Jeong, J. Son, J. Jeong, J. Jin, Proc. SPIE 10727 (2018) 107270W.
[3] T.A. Growden, W. Zhang, E.R. Brown, D.F. Storm, et al., Light Sci. Appl. 7 (2018) 17150.
[4] A. Yoshikawa, S. Ushida, K. Nagase, M. Iwaya, et al., Appl. Phys. Lett. 111 (2017) 191103.
[5] Y.R. Chen, Z.W. Zhang, H. Jiang, Z.M. Li, G.Q. Miao, H. Song, J. Mater. Chem. C 6 (2018) 4936–4942.
[6] M. Takeuchi, H. Shimizu, R. Kajitani, K. Kawasaki, et al., J. Cryst. Growth 305 (2007) 360–365.
[7] S.R. Lee, A.M. West, A.A. Allerman, K.E. Waldrip, et al., Appl. Phys. Lett. 86 (2005) 241904.
[8] W.Y. Han, Z.W. Zhang, Z.M. Li, Y.R. Chen, H. Song, et al., J Mater. Sci. 29 (2018) 9077–9082.
[9] K. Ahadi, H. Kim, S. Stemmer, APL Mater. 6 (2018) 056102.
[10] S. Lim, Y. Ko, C. Rodriguez, S. Gong, Y. Cho, Light Sci. Appl. 5 (2016) e16030.
[11] K. Ahadi, X.Z. Lu, S. Saknabu-Rezaie, P.B. Marshall, J.M. Rondinelli, et al., Phys. Rev. B 99 (2019) 041106.
[12] S.B. Li, M.E. Ware, J. Wu, P. Minor, Z.M. Wang, et al., Appl. Phys. Lett. 101 (2012) 122103.
[13] E. Matioli, S. Brinkley, K.M. Kelchner, Y. Hu, S. Nakamura, et al., Light Sci. Appl. 1 (2012) e22.